A Generalized Computationally Efficient Inverse Characterization Approach Combining Direct Inversion Solution Initialization with Gradient-Based Optimization

Mengyu Wang[b,c], John C. Brigham[a,c,*]

[a]*School of Engineering and Computing Sciences, Durham University, Durham, UK*
[b]*Schepens Eye Research Institute, Harvard Medical School, Boston, USA*
[c]*Department of Civil and Environmental Engineering, University of Pittsburgh, Pittsburgh, USA*

Abstract

A computationally efficient gradient-based optimization approach for inverse material characterization from incomplete system response measurements that can utilize a generally applicable parameterization (e.g., finite element-type parameterization) is presented and evaluated. The key to this inverse characterization algorithm is the use of a direct inversion strategy with Gappy proper orthogonal decomposition (POD) response field estimation to initialize the inverse solution estimate prior to gradient-based optimization. Gappy POD is used to estimate the complete (i.e., all components over the entire spatial domain) system response field from incomplete (e.g., partial spatial distribution) measurements obtained from some type of system testing along with some amount of *a priori* information regarding the potential distribution of the unknown material property. The estimated complete system response is used within a physics-based direct inversion procedure with a finite element-type parameterization to estimate the spatial distribution of the desired unknown material property with minimal computational expense. Then, this estimated spatial distribution of the unknown material property is used to initialize a gradient-based optimization approach, which

---

[*]Corresponding author
Email addresses: `mengyu_wang@meei.harvard.edu` (Mengyu Wang),
`john.brigham@durham.ac.uk` (John C. Brigham)

uses the adjoint method for computationally efficient gradient calculations, to produce the final estimate of the material property distribution. The three-step ((1) Gappy POD, (2) direct inversion, and (3) gradient-based optimization) inverse characterization approach is evaluated through simulated test problems based on the characterization of elastic modulus distributions with localized variations (e.g., inclusions) within simple structures. Overall, this inverse characterization approach is shown to efficiently and consistently provide accurate inverse characterization estimates for material property distributions from incomplete response field measurements. Moreover, the solution procedure is shown to be capable of extrapolating significantly beyond the initial assumptions regarding the potential nature of the unknown material property distribution.

---

1. Introduction

Computational methods for the solution of inverse problems (e.g., characterization, design, etc.) in mechanics (e.g., relating to solid mechanics, heat transfer, etc.) are becoming ever more popular in a variety of fields in science and engineering. In particular, applications in the characterization of material property distributions span interest areas from civil engineering (e.g., structural damage characterization [1, 2]) to medicine (e.g., tissue characterization for disease diagnosis [3, 4]), where quantitative estimation of a variety of material parameters can provide critical information relating to the state of the system. A common structure of quantitative inverse material characterization approaches is to couple a numerical representation of the system forward problem (e.g., a finite element representation of the system response given the material properties) with some type of optimization to estimate the material properties that lead to a "best match" between the response estimated by the forward numerical representation and the available experimentally measured response. Such computational methods to estimate inverse solutions provide quantitative solutions and are generally applicable regardless of the physics of interest and response measurement type. However, there are several significant challenges depending on the application of

2

interest as well, with a wide range of variations in the inverse solution method specifics. Common differences include variations in the parameterization of the unknown material field, numerical analysis technique, and optimization approach, with each having significant tradeoffs in terms of generalization of the applicability, solution accuracy, and computational efficiency.

One way in which computational inverse solution strategies can be divided is into those that are iterative and those that are non-iterative (i.e., direct). A common direct approach is to relate the measured response to the unknown material property distribution parameters based on the manipulation of the forward boundary value problem and a least-squares criteria, which creates a solution process similar to that of solving the forward problem itself (e.g., similar in process to a finite element analysis to predict the deformation response of a solid given geometry, material properties, and boundary conditions) [5, 6, 7]. Thus, the solution estimate can be obtained at a cost on the order of a single numerical analysis of the forward problem, even with a relatively generalized parameterization of the spatial distribution of the unknown property (e.g., finite element-type parameterization). However, one common challenge of the direct inversion approaches is that the entire (or nearly entire) spatial distribution (i.e., full-field) of the system response (e.g., displacement) must be measured to successfully characterize a distribution of unknown material properties. In addition, direct approaches are often relatively noise sensitive, with solution quality degrading relatively quickly with increasing levels of measurement noise.

Iterative optimization-based approaches are typically better equipped than direct methods to estimate inverse solutions provided with response measurements from only a portion of the system domain (i.e., partial-field measurements) or otherwise incomplete measurement information (e.g., single directional components of displacement). Conceptually these iterative approaches can be further divided into those that use non-gradient-based optimization (e.g., random search, genetic algorithm, etc.) [8, 9] and those that use gradient-based optimization (e.g., Newton's method, conjugate gradient, etc.) [4, 10]. Non-gradient-based methods often have more significant global search capabilities in comparison to the gradient-based optimization approaches, which can become trapped in local minima (i.e., an inaccurate solution). However, non-gradient-based methods typically require substantially more iterations (i.e., computational time) to converge to a solution approximation than gradient-based approaches, which can be prohibitive for many applications. Moreover, the computational expense of non-gradient-

based methods increases substantially with increasing number of unknown parameters (i.e. the curse of dimensionality), leading to the use of simplified (i.e., less generally applicable) parameterizations of the unknown property field. In contrast, gradient-based methods are not only substantially more computationally efficient overall, but are also not as affected by the curse of dimensionality, particularly if using an adjoint approach or something similar to calculate the gradients [11, 12, 13]. Therefore, gradient-based methods are capable of converging to a solution estimate with relative computational efficiency, even with a generally applicable high-dimensional finite-element type parameterization of the unknown material property field. Unfortunately, as stated, gradient-based methods are local in nature, and unless the initial estimate of the unknown property field provided is relatively accurate, the final solution estimate is likely to be inaccurate. Furthermore, limitations in the amount of measurement data and/or high-dimensional parameterizations of the unknown field often leads to complicated (non-convex) error surfaces for the optimization, and while regularization approaches can somewhat relieve this challenge [14, 4, 15], the importance of the initial estimate accuracy is increased significantly.

The present work investigates an approach to utilize information that is available *a priori* regarding the nature of the unknown property distribution (e.g., that the distribution has localized variations) to initialize a gradient based optimization procedure to achieve a unique level of efficiency and accuracy to estimate generalized (i.e., arbitrarily shaped) distributions of material properties from partial-field measurements without the need for regularization or any kind of direct initial solution estimate. This work is a direct extension of the prior work of the authors that displayed the capability of a highly computationally efficient direct inversion characterization strategy using Gappy proper orthogonal decomposition (POD) [16]. The prior work showed the promise of using Gappy POD to significantly improve the quality of direct inversion characterization solution estimates without significant additional computing cost (particularly in terms of the online portion of the process). Alternatively, the present work shows the capability to improve solution quality even further by utilizing this Gappy POD-direct inversion approach to initialize a gradient-based optimization process. In particular, the approach is presented in the context of characterizing the spatial distribution of the elastic modulus (i.e., elastography) provided with displacement response measurements over some portion of the solid domain. The approach utilizes the Gappy POD machine learning technique to build a data recon-

4

struction tool based on the available *a priori* solution knowledge that can estimate the full-field response distribution given the available partial-field measurements. The estimated full-field response is then applied within a direct inversion strategy with a general finite element-type parameterization of the unknown field to produce an initial estimate of the spatial distribution of the unknown material property over the entire domain. Lastly, this initial estimate is refined with a gradient-based optimization strategy using the adjoint method for computationally efficient gradient calculations to produce the final estimate of the material property distribution.

The following section presents the details of the inverse material characterization algorithm, including (1) the description of the gradient-based optimization approach with adjoint method, (2) the Gappy POD approach to reconstruct a full-field response estimate from given partial-field measurements, and (3) the direct inversion algorithm to estimate the spatial distribution of elastic modulus provided with the full-field displacement response distribution reconstructed from Gappy POD and the boundary conditions corresponding to the test method used to produce the measurements. Then, simulated examples relating to characterization of localized elastic modulus distributions in solids are presented to examine the capabilities of the generalized inverse characterization approach, which is followed by the concluding remarks.

2. Inverse Material Characterization Algorithm

2.1. Optimization-Based Inversion

As discussed, although potentially applicable to a variety of different physical systems, material properties, and testing methods, the inverse characterization approach is presented in the specific context of characterization of the elastic modulus spatial distribution of a solid from partial-field displacement measurements. In particular, for the following presentation, it is assumed that some type of steady-state dynamic mechanical testing has been applied, with the solid of interest excited to steady state at one or more excitation frequencies and the resulting steady-state displacement amplitude measured at several locations throughout the solid. Thus, neglecting body forces and damping, assuming displacements and strains are small, and assuming that the system variables vary harmonically in time at angular excitation frequency ω, the steady-state dynamic governing equations describing

5

the associated forward elasticity problem (i.e., the strong form) can be given as:

$$\nabla \cdot \boldsymbol{\sigma}(\boldsymbol{x}, \omega) + \omega^2 \rho(\boldsymbol{x}) \boldsymbol{u}(\boldsymbol{x}, \omega) = \boldsymbol{0}, \quad \forall \boldsymbol{x} \in \Omega, \tag{1}$$

$$\boldsymbol{\sigma}(\boldsymbol{x}, \omega) = \boldsymbol{C}^{IV}(\boldsymbol{x}) : \boldsymbol{\varepsilon}(\boldsymbol{x}, \omega), \tag{2}$$

$$\boldsymbol{\varepsilon}(\boldsymbol{x}, \omega) = \frac{1}{2} \left(\nabla \boldsymbol{u}(\boldsymbol{x}, \omega) + (\nabla \boldsymbol{u}(\boldsymbol{x}, \omega))^T \right), \tag{3}$$

$$\boldsymbol{\sigma}(\boldsymbol{x}, \omega) \cdot \boldsymbol{n}(\boldsymbol{x}) = \boldsymbol{T}(\boldsymbol{x}, \omega), \quad \forall \boldsymbol{x} \in \Gamma_{\boldsymbol{T}}, \tag{4}$$

and

$$\boldsymbol{u}(\boldsymbol{x}, \omega) = \boldsymbol{u}_0(\boldsymbol{x}, \omega), \quad \forall \boldsymbol{x} \in \Gamma_{\boldsymbol{u}}, \tag{5}$$

where $\rho(\boldsymbol{x})$ is the mass density, $\boldsymbol{\sigma}(\boldsymbol{x}, \omega)$ is the Cauchy stress amplitude tensor, $\boldsymbol{u}(\boldsymbol{x}, \omega)$ is the displacement amplitude vector, Ω is the domain of the structure, $\boldsymbol{\varepsilon}(\boldsymbol{x}, \omega)$ is the small strain amplitude tensor, $\boldsymbol{C}^{IV}(\boldsymbol{x})$ is the 4th-order elasticity tensor, $\boldsymbol{n}(\boldsymbol{x})$ is the unit outward normal vector to the surface of the domain, $\boldsymbol{T}(\boldsymbol{x}, \omega)$ and $\Gamma_{\boldsymbol{T}}$ are the applied traction amplitude vector and the portion of the domain surface where this traction is applied, respectively, and $\boldsymbol{u}_0(\boldsymbol{x}, \omega)$ and $\Gamma_{\boldsymbol{u}}$ are the applied displacement amplitude vector and the portion of the domain surface where displacement is known, respectively. Note that the entire formulation is applicable and easily converted to the static case by simply setting the momentum term to zero.

The first step in setting up the optimization-based computational inverse solution procedure is to construct an appropriate objective functional. This objective functional should somehow quantify the difference between the experimentally measured system response and the corresponding response that is predicted by the numerical representation of the system (i.e., solution to Eqns. (1)-(5)) given an estimate to the unknown material properties, as (note that dependencies on $\boldsymbol{x}$ and ω should be inferred and were left off of the following presentation for brevity):

$$f(\boldsymbol{p}) = \left\| \boldsymbol{u}(\boldsymbol{p}) - \boldsymbol{u}^M \right\|_{\Omega^M}, \tag{6}$$

where, for this example, $\boldsymbol{u}^M$ would be the experimentally measured displacement amplitudes, $\boldsymbol{u}(\boldsymbol{p})$ is the numerical simulated displacement amplitudes for a given estimate to the material parameter vector, $\boldsymbol{p}$, and $\|\cdot\|_{\Omega^M}$ is some chosen suitable metric norm that combines the contribution of all measurement locations and excitation frequencies to produce a scalar measurement error. Then, all that is necessary is to apply a suitable optimization algorithm, to minimize the objective functional, f, with respect to the unknown

6

material parameters, subject to the constraint of the above boundary value problem (BVP) and any physical bounds on the unknown parameters. There are several different gradient-based optimization algorithms that can be (and have been in prior studies [17]) applied to minimize the objective functional with respect to the unknown material parameters, and thereby, estimate the inverse problem solution. For example, the standard interior point method was used for the examples presented herein, which among other algorithmic details that can be found in [18], uses the gradient to approximate the inverse of the Hessian with a BFGS method [17] to update the solution estimate at each iteration. Therefore, much like many other commonly used gradient-based optimization algorithms, the gradient is the main driver of the optimization, and therefore, the most critical calculation within the optimization procedure.

By far the most challenging aspect (at least computationally) of calculating the gradient of the objective functional presented above is the need to calculate the partial derivative of the displacement response with respect to the material parameters ($\boldsymbol{p}$), with the relationship between those two quantities being defined by the above BVP. As such, to maintain computational efficiency, the present work used the adjoint method for the gradient calculation [15]. The adjoint method requires only two numerical solutions of BVPs to calculate the necessary gradient, the given BVP and a corresponding adjoint BVP, with both having the same approximate computational expense. Therefore, the adjoint method represents a substantial computational savings in comparison to alternate methods, such as finite difference methods, which require at least $N + 1$ BVP solutions, or direct differentiation of the BVP, which requires N BVP solutions, where N is the number of unknown parameters in the optimization problem [4]. Particularly for generalized (e.g., finite element-type) parameterizations of the unknown property with large numbers of parameters to be determined, the adjoint method, or something similar, is a necessity for practical applicability.

As discussed in the Introduction, providing a sufficiently accurate initial guess for the unknown material parameters is critical to ensuring an accurate final solution estimate using the computational inverse characterization procedure with gradient-based optimization. The importance of this initial guess is even further heightened when applying a generalized parameterization of the unknown field and when not using any kind of solution regularization (as is the case in the above presentation). To overcome this challenge/limitation, the present work uniquely uses a direct inversion strategy to estimate an ini-

7

tial guess for the unknown material property distribution, which is detailed in the following.

2.2. Direct Inversion with Gappy POD

Overall, the procedure to obtain an initial material distribution estimate provided with partial field measurement data involves first applying the Gappy POD machine learning tool to reconstruct a full-field estimate of the measurement data. Then this full-field measurement estimate is used to directly invert the governing equations describing the physics of the tested system to estimate the unknown material property distribution. Details of this Gappy POD-direct inversion approach utilized for obtaining an initial estimate of the unknown material property distribution can be found in the prior work of the authors [16], and only key points are discussed briefly herein.

Gappy POD is an extension of the traditional POD approach that was first developed and presented by Everson and Sirovich [19] for the purpose of filling in missing information to reconstruct marred photos. Subsequently, Gappy POD has shown substantial capabilities to accurately reconstruct physical processes from partial-field measurement data, especially for fluid flow problems [20, 21, 22, 23, 24].

The Gappy POD process begins with the standard POD method. Given a set of n fields (referred to as "snapshots"), $\{\boldsymbol{u}_k(\boldsymbol{x})\}_{k=1}^{n}$, POD can be interpreted as an approach to determine the set of m orthogonal basis functions (i.e., modes), $\{\boldsymbol{\phi}_i(\boldsymbol{x})\}_{i=1}^{m}$, that are optimal in the average L_2-error sense for representing each given field and, if the given fields are representative, any similar field as:

$$\boldsymbol{u}(\boldsymbol{x}) \approx \boldsymbol{u}^*(\boldsymbol{x}) = \sum_{i=1}^{m} a_i \boldsymbol{\phi}_i(\boldsymbol{x}), \qquad (7)$$

where a_i is the modal coefficient corresponding to the i^{the} mode ($\boldsymbol{\phi}_i(\boldsymbol{x})$). Then, the POD optimization problem to define these modes can be written as:

$$\underset{\{\boldsymbol{\phi}_i(\boldsymbol{x})\}_{i=1}^{m}}{Minimize} \left\langle \|\boldsymbol{u}(\boldsymbol{x}) - \boldsymbol{u}^*(\boldsymbol{x})\|_{L_2(\Omega)}^2 \right\rangle, \qquad (8)$$

where

$$\langle \boldsymbol{u} \rangle = \frac{1}{n} \sum_{k=1}^{n} \boldsymbol{u}_k, \qquad (9)$$

and $\boldsymbol{u}^*$ is the best approximation of the snapshots from the modes (i.e., the projection of each snapshot onto the modes). Based on this optimization

problem and applying the method of snapshots (see [25] for additional details), a maximum of n POD modes can be calculated through the solution of the following eigenvalue problem:

$$\frac{1}{n} \sum_{k=1}^{n} A_{jk} C_k = \lambda C_j, \tag{10}$$

where

$$A_{jk} = \int_{\Omega} \boldsymbol{u}_j(\boldsymbol{x}) \cdot \boldsymbol{u}_k(\boldsymbol{x}) \, d\boldsymbol{x}, \tag{11}$$

and then the ith mode is given as:

$$\boldsymbol{\phi}_i(\boldsymbol{x}) = \frac{1}{\lambda^{(i)} n} \sum_{k=1}^{n} \boldsymbol{u}_k(\boldsymbol{x}) C_k^{(i)}. \tag{12}$$

Gappy POD diverges from standard POD in how the modes are utilized. If the full spatial distribution of a field is available, the modal coefficients (a_i) needed to reconstruct that field with the POD modes can be easily obtained by projecting the modes onto the field as:

$$a_i = \int_{\Omega} \boldsymbol{u}(\boldsymbol{x}) \cdot \boldsymbol{\phi}_i(\boldsymbol{x}) \, d\boldsymbol{x}. \tag{13}$$

Alternatively, the objective of Gappy POD is to provide a means to reconstruct the full spatial distribution of a field using the POD modes, but with only a partial spatial distribution of the field given. Defining $\hat{\boldsymbol{u}}(\boldsymbol{x})$ as the given partial distribution of the field of interest such that $\hat{\boldsymbol{u}}(\boldsymbol{x})$ is (incorrectly) 0 anywhere data is unavailable, then $\hat{\boldsymbol{u}}(\boldsymbol{x})$ can be expressed in terms of the corresponding, but unknown, full spatial distribution as:

$$\hat{\boldsymbol{u}}(\boldsymbol{x}) = \beta(\boldsymbol{x}, \boldsymbol{u}) \boldsymbol{u}(\boldsymbol{x}), \tag{14}$$

where $\beta(\boldsymbol{x}, \boldsymbol{u})$ is a mask function that is defined as 0 where data is unavailable and 1 where data is available. Assuming that the full spatial distribution can be approximated with the POD modes as defined in Eqn. (7), an approximation of $\hat{\boldsymbol{u}}(\boldsymbol{x})$ can be written in terms of the POD modes as:

$$\hat{\boldsymbol{u}}^*(\boldsymbol{x}) = \beta(\boldsymbol{x}, \boldsymbol{u}) \sum_{i=1}^{m} a_i \boldsymbol{\phi}_i(\boldsymbol{x}). \tag{15}$$

9

Then, based upon a least-squares criteria, the optimal set of modal coefficients to reconstruct the full spatial distribution of the field can be defined as that which minimizes an error function of the form:

$$\varepsilon = \int_\Omega \left[\beta\left(\boldsymbol{x}, \boldsymbol{u}\right) \boldsymbol{u}\left(\boldsymbol{x}\right) - \beta\left(\boldsymbol{x}, \boldsymbol{u}\right) \sum_{i=1}^{m} a_i \boldsymbol{\phi}_i(\boldsymbol{x}) \right]^2 d\boldsymbol{x}. \tag{16}$$

Applying the necessary condition for extrema of a function by setting the derivative of the error function with respect to the modal coefficients to zero, the optimal set of modal coefficients, {a}, to reconstruct the full spatial distribution of the field can be determined from the solution of:

$$\boldsymbol{M}\boldsymbol{a} = \boldsymbol{f}, \tag{17}$$

where

$$M_{ij} = \int_\Omega \beta\left(\boldsymbol{x}, \boldsymbol{u}\right) \boldsymbol{\phi}_i(\boldsymbol{x}) \cdot \boldsymbol{\phi}_j(\boldsymbol{x}) \; d\boldsymbol{x}. \tag{18}$$

and

$$f_i = \int_\Omega \beta\left(\boldsymbol{x}, \boldsymbol{u}\right) \boldsymbol{u}(\boldsymbol{x}) \cdot \boldsymbol{\phi}_i(\boldsymbol{x}) \; d\boldsymbol{x}. \tag{19}$$

A last important implementation aspect for this Gappy POD approach is that only a portion ($m \ll n$) of the set of modes that can be obtained with POD are typically necessary to be retained for further use in the full-field estimation process. As the associated eigenvalues from the solution of Eqn. (10) relate to the value of each mode for the representation of the given dataset, typically some heuristic is used based on the relative sum of the associated eigenvalues to determine the modes to retain for further use [21, 22].

One additional note is that the Gappy POD approach can also act as somewhat of a noise filter during the reconstruction process, thereby providing an added benefit of reducing the effects of measurement noise on the subsequent direct inversion solution procedure. However, any reconstructed full-field response is still only an approximation of the true full-field response, with the accuracy of the response estimation and direct inversion solution estimate significantly dependent upon the amount of measurement data (higher accuracy with more data).

The direct inversion procedure utilized herein (discussed in the context of elastography) first assumes that the elastic modulus distribution can be

approximated in a finite element format similar to the format of the standard displacement approximation [16]. Thus, utilizing the full-field solution estimate provided by Gappy POD and applying a standard weak form Galerkin procedure, the finite element equations for the direct inversion elastography problem to determine nodal values describing the elastic modulus ($\boldsymbol{E}$) from the nodal values describing the full-field displacement response ($\boldsymbol{u}$) can be written as:

$$\boldsymbol{K_I E} = \boldsymbol{P_I} + \boldsymbol{M_I u}, \tag{20}$$

where

$$\boldsymbol{K_I} = \sum_{element} \int_{\Omega^e} [B_{\delta\boldsymbol{E}}(\boldsymbol{x})]^T [D_I][B_{\boldsymbol{u}}(\boldsymbol{x})]\{\boldsymbol{u}^e\}[N_E(\boldsymbol{x})] \ d\boldsymbol{x}, \tag{21}$$

$$\boldsymbol{M_I} = \sum_{element} \int_{\Omega^e} \rho(\boldsymbol{x})\omega^2 [N_{\delta\boldsymbol{E}}(\boldsymbol{x})]^T [N_{\boldsymbol{u}}(\boldsymbol{x})] \ d\boldsymbol{x}, \tag{22}$$

$$\boldsymbol{P_I} = \sum_{element} \int_{\Gamma^e_{\boldsymbol{T}}} [N_{\delta\boldsymbol{E}}(\boldsymbol{x})]^T \boldsymbol{T}(\boldsymbol{x}, \omega) \ d\boldsymbol{x}, \tag{23}$$

$\boldsymbol{D_I}$ is is the matrix derived from the elasticity matrix $\boldsymbol{D}$ (i.e., the Voigt notation version of $\boldsymbol{C}^{IV}$) after separating the elastic modulus ($E(\boldsymbol{x})$) (i.e., $\boldsymbol{D} = \boldsymbol{D_I} E(\boldsymbol{x})$), $\boldsymbol{N_E(x)}$ is the matrix of shape functions for elastic modulus interpolation, $\boldsymbol{N_{\delta E}(x)}$ is the expanded version (to match the dimensions of the displacement) of the matrix of shape functions for elastic modulus interpolation, $\boldsymbol{N_u(x)}$ is the standard matrix of shape functions for displacement interpolation, and $\boldsymbol{B_E(x)}$, $\boldsymbol{B_{\delta E}(x)}$, and $\boldsymbol{B_u(x)}$ are the respective matrices of these shape function spatial derivatives. Lastly, a least-squares approach can be applied to solve the non-square system described by Eqn. (20), such that the nodal values of elastic modulus can be determined as:

$$\boldsymbol{E} = \left(\boldsymbol{K_I^T K_I}\right)^{-1} \boldsymbol{K_I^T} \left(\boldsymbol{P_I} + \boldsymbol{M_I u}\right). \tag{24}$$

One final important point is that it is necessary to eliminate the equations corresponding to the essential boundary conditions in the forward BVP prior to the solution of Eqn. (24). Eliminating these equations is a common approach that is necessary to obtain a well-behaved solution to the direct inversion problem. Thus, prior to solving Eqn. (24) the rows in Eqn. (20) corresponding to nodes where essential boundary conditions are present are set to zero, such that:

$$\boldsymbol{K_I}[i, :] = 0, \ \ \text{if} \ \ \boldsymbol{x}_i \in \Gamma_{\boldsymbol{u}}, \ \ \text{for} \ \ i = 1, 2, ..., N, \tag{25}$$

11

$$\boldsymbol{M_I u}[i] = 0, \quad \text{if} \quad \boldsymbol{x}_i \in \Gamma_{\boldsymbol{u}}, \quad \text{for} \quad i = 1, 2, ..., N, \tag{26}$$

and

$$\boldsymbol{P_I}[i] = 0, \quad \text{if} \quad \boldsymbol{x}_i \in \Gamma_{\boldsymbol{u}}, \quad \text{for} \quad i = 1, 2, ..., N. \tag{27}$$

2.3. Algorithm for Inverse Material Characterization Combining Direct Inversion and Optimization-Based Inversion

The three-step ((1) Gappy POD, (2) direct inversion and (3) gradient-based optimization) inverse material characterization algorithm can be summarized as follows:

Given: The structure geometry, boundary conditions, and partial field measurements from a nondestructive test, and any available material properties.

Find: The unknown material property distribution.

Step 1: Sample a set of potential distributions for the unknown material property and generate corresponding full-field structural responses under the nondestructive testing conditions.

Step 2: Calculate the POD modes from the set of full-field structural responses and select the modes to be retained based on eigenvalue energy.

Step 3: Reconstruct the full-field structural response from the given partial-field measurements with Gappy POD.

Step 4: Direct inversion for the unknown material property distribution with reconstructed full-field structural response.

Step 5: Apply gradient-based optimization to further improve the initial estimate of material property distribution provided by direct inversion with Gappy POD.

3. Examples and Discussion

Two sets of numerically simulated inverse characterization problems were considered to evaluate the potential benefits and capabilities of the gradient-based optimization approach initialized with direct inversion from Gappy POD response approximation. Both example sets involved characterization of an elastic modulus distribution with localized inclusions (hard or soft)
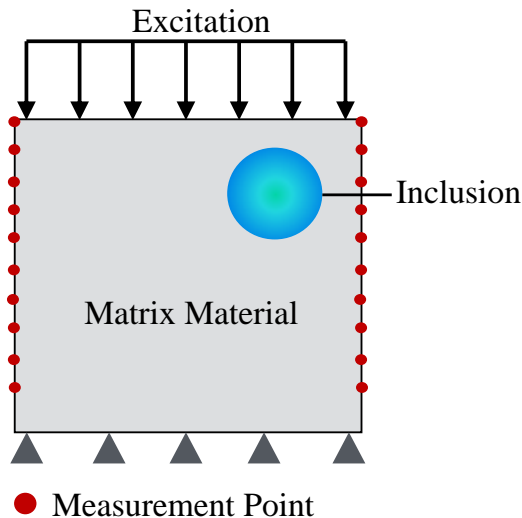
Figure 1: Schematic for the numerically simulated examples representing characterization of an elastic modulus distribution with an inclusion based on mechanical testing involving the excitation and measurement points shown.

in plate structures from partial-field response measurements. Furthermore, both inverse characterization problems were based upon some type of simulated nondestructive testing (dynamic or static) in the linear range of the solid behavior (such that the governing equations shown in Section 2 apply), with an actuation force applied uniformly to the top surface, the bottom surface fixed, and with the horizontal and vertical displacement response to the loading measured at 10 uniformly spaced discrete locations on both the left and right surfaces. Fig. 1 shows a schematic of the example cases, including the boundary conditions and sensor locations.

The "experimental" nondestructive test measurements were simulated using the standard finite element method. Furthermore, triangular elements with quadratic interpolation were used, and the mesh was ensured to be sufficiently refined to provide accurate results for the problem space considered. In addition, both examples used the plane stress assumption to reduce the computational expense. To add realism to the simulated experiments, for all trials 1% Gaussian white noise was also added to the simulated measurements as:

$$u^{expn} = u^{exp} \left(1 + 0.01 v\right), \tag{28}$$

where u^{expn} and u^{exp} are the simulated experimental displacement measure-

ments with noise and without noise, respectively, and υ is a normally distributed random variable with unit variance and zero mean. Note that testing (not shown here for brevity) showed a significant tradeoff between the level of noise and the amount of measurement information in terms of the final solution accuracy. The testing showed that the more measurement information (i.e., the more sensor locations) the more tolerant the inverse solution procedure would be to measurement noise.

It was assumed that *a priori* knowledge would be available that the elastic modulus distributions to be characterized in the examples would be localized (e.g., as could be expected in applications of damage characterization of civil structures [26] or tumor characterization of biological structures [13]). As such, the snapshot response fields used for the Gappy POD procedure were generated using a Gaussian radial basis function (RBF) representation of the elastic modulus (see [27, 28, 29] for other similar works utilizing a RBF representation to define localized elastic modulus variations), as:

$$E(\boldsymbol{x}) = E_0 \left[1 + \alpha \cdot exp \left(-\frac{(\boldsymbol{x} - \boldsymbol{c})^2}{r^2} \right) \right],$$ (29)

where E_0 is the elastic modulus of the matrix material, α is the relative change in elastic modulus at the inclusion center, $\boldsymbol{c}$, is the location of the inclusion center, and r is the breadth of the inclusion. Note, as will be shown in the following example cases, although snapshots were generated based upon single circular inclusion cases (defined by Eqn. (29)), the approach presented is capable of being applied to substantially more complicated cases (e.g., multiple inclusions and/or irregularly shaped inclusions).

The finite element method was again used to generate all snapshots for the POD process. In addition, the criteria used to determine the number of modes (m) out of the total number available (n) to use for data reconstruction with Gappy POD was to select the mode with the highest associated eigenvalue λ as well as the minimum number of the remaining modes, such that:

$$\frac{\sum_{j=2}^{m} \lambda^{(j)}}{\sum_{i=2}^{n} \lambda^{(i)}} \times 100\% > 99.9\%$$ (30)

This criteria was determined to be sufficient to ensure that enough modes were retained from POD for Gappy POD to produce accurate reconstructions, while excluding the modes associated with low eigenvalues that can often cause the matrix $[M]$ in Eqn. (17) to be ill-conditioned.

14

The specific objective function used for the gradient-based optimization procedure to estimate the inverse solutions in both examples was the square of the l_2-error as:

$$f(\boldsymbol{p}) = \|\boldsymbol{u}\left(\boldsymbol{p}\right) - \boldsymbol{u}^{expn}\|_{l_2}^2, \tag{31}$$

In addition, the same finite element-type parameterization of the unknown elastic modulus distribution was utilized for both the direct inversion and subsequent gradient-based optimization processes (note that all meshes, including both the forward and inverse problems, were verified to be sufficiently refined for accurately analyzing all potential system responses and material property distributions). As noted previously, the interior point optimization method [18] was the specific gradient-based optimization algorithm chosen, with the adjoint method utilized to calculate the necessary gradient at each iteration, to minimize the associated objective function and estimate the solution to the example inverse characterization problems. The scientific analysis software MATLAB [30] was used to implement the interior point method, largely with default settings, including calculation of the Hessian with a dense quasi-Newton approximation in which both Newton steps and conjugate gradient steps were both allowed at each iteration. For all cases, the stopping criteria was set to 50 iterations, which was sufficient for convergence.

3.1. Example 1: Steady-State Dynamic Test of Hard Matrix with Soft Inclusions

The first example consisted of a simulated $1\ m \times 1\ m$ aluminum plate. The entire material (matrix and inclusions) was assumed to be known to have a Poisson's ratio of 0.3 and a density of 2700 kg/m^3. The simulated steady-state dynamic test was implemented by applying the harmonic excitation at a frequency of 20 Hz and amplitude of 1 kN/m (factoring out the arbitrary thickness) uniformly to the top surface of the plate. This particular scenario could be relevant to applications in nondestructive evaluation of civil or aerospace structures (e.g., characterizing damage in structural components as could be represented by a reduction in stiffness) from frequency response-based testing.

For the process of generating the snapshots for POD, the elastic modulus of the background material (i.e., matrix material) was assumed to be fixed at 69.0 GPa. Alternatively, the parameters defining the inclusion based on the RBF description were assumed to be variable. The specific parameter values
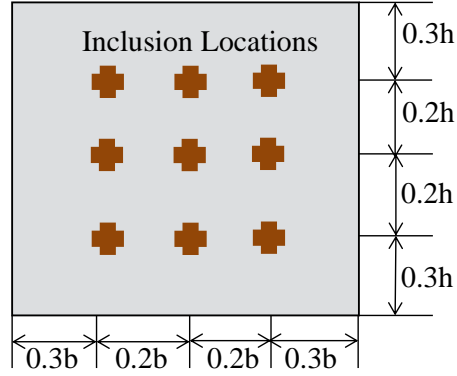
Figure 2: Schematic of the nine inclusion centers used separately to generate the snapshots for POD for the numerically simulated examples.

used to create the snapshots were chosen arbitrarily by uniformly sampling the space of the four variable parameters (the two spatial coordinates, amplitude, and breadth). Three values were chosen for each spatial coordinate of the inclusion center and two values were chosen each for the amplitude and breadth of the inclusion, and one last scenario with no inclusion (i.e., homogeneous matrix material) was added, for a total of 37 parameter combinations used to create snapshots. Fig. 2 shows the nine location combinations of the inclusion center used to generate the snapshots. The values of the other two parameters used to create the parameter combinations were chosen based on an expectation of what the lower and upper-end would be for the application, using -0.3 and -0.7 for the amplitude parameter α (i.e., modulus at soft inclusion center of 21 GPa and 48 GPa) and 0.1 m and 0.3 m for the breadth parameter r. To be clear, again note that each of elastic modulus distribution realizations used to create a snapshot contained only one inclusion (other than the homogeneous case, which contained none). 13 out of the 37 total available POD modes were necessary to satisfy the criteria defined in Eqn. 30 and were retained for the Gappy POD reconstruction process. Also note that to provide a fair evaluation of the methods presented, none of the modulus distributions considered in the test cases matched the modulus distributions used to generate the snapshots.

3.1.1. Case 1 Results: Single Circular Inclusion

First, the case of a single circular inclusion within the simulated aluminum plate was examined. A preliminary analysis was done to provide some direc-
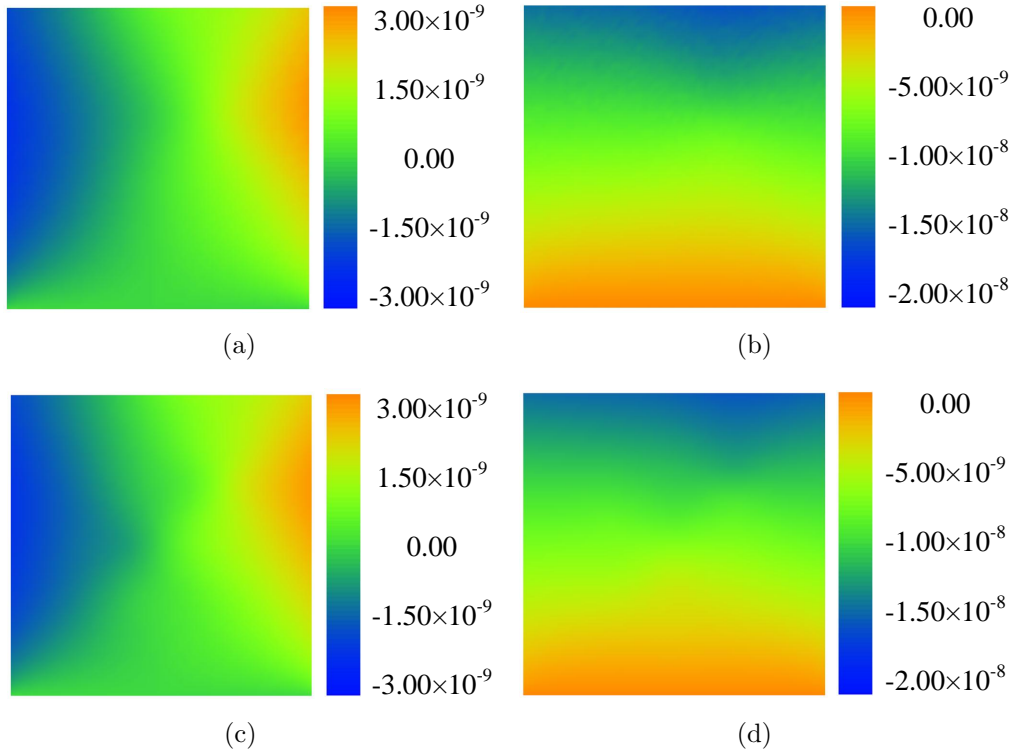
16

Figure 3: Representative single circular inclusion example of the (a) horizontal and (b) vertical components of a simulated experimental displacement field with 1% Gaussian white noise and the (c) horizontal and (d) vertical components of the corresponding reconstructed full-field displacement from Gappy POD with the partial-field measurements for the simulated aluminum plate example (color contours are in units of m).

t perspective on the capability of the Gappy POD process to estimate the full-field displacement response from the 20 measurement locations provided. Fig. 3 shows a representative example of a full-field simulated response including the 1% Gaussian white noise (i.e., the "true response") for a randomly generated single-inclusion elastic modulus distribution in comparison to the full-field displacement estimation from the 20 measurements of this noisy simulated response with the Gappy POD procedure. The relative L_2 and L_∞ errors over the entire domain of this displacement reconstruction in contrast to the true displacement response are 1.8% and 5.0%, respectively. As such, the analysis of the full-field response estimation procedure showed that the Gappy POD approach could reconstruct such a displacement response from partial field measurements with a relatively high level of
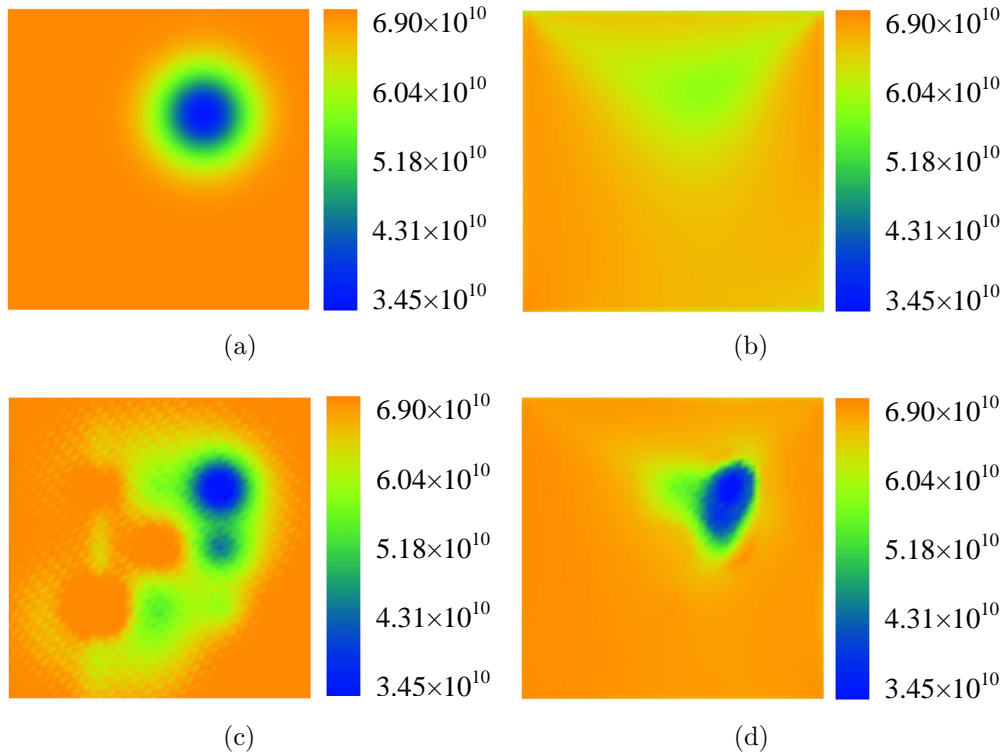
17

Figure 4: Representative single circular inclusion example of (a) the target elastic modulus distribution, (b) the elastic modulus distribution estimated with gradient-based optimization initialized with a homogeneous material distribution, (c) the elastic modulus distribution estimated with the direct inversion approach with Gappy POD full-field displacement reconstruction, and (d) the elastic modulus distribution estimated with gradient-based optimization initialized with the direct inversion solution for the simulated aluminum plate example (color contours in units of Pa).

accuracy.

Next, the complete inverse characterization procedure with Gappy POD response estimation, direct inversion, and gradient-based optimization was examined. Fig. 4 shows a representative example of a randomly generated single-inclusion elastic modulus distribution used to simulate experimental measurements (i.e., the "target distribution"), the corresponding elastic modulus distribution estimated by the direct inversion procedure with Gappy POD full-field response estimation (i.e., the initial guess for the gradient based optimization), and the corresponding final elastic modulus distribution estimation from the subsequent gradient-based optimization. In addition, to

provide a baseline, Fig. 4 also shows results from an attempt to estimate the elastic modulus distribution applying the gradient-based optimization procedure with a homogeneous (i.e., no inclusion) elastic modulus distribution as the initial solution guess (as would be a natural selection without any other information provided), rather than using the results of the direct inversion as the initial guess. It is clear that without the direct inversion-Gappy POD initialization procedure, the gradient-based optimization is entirely ineffectual at providing an accurate estimation of the inverse problem solution, not even qualitatively indicating the presence of an inclusion. Alternatively, the direct inversion with Gappy POD was capable of a significantly more accurate estimation of the elastic modulus distribution, clearly identifying the presence of an inclusion, but still with an erroneous prediction of dispersed softening throughout the domain. Finally, the application of the gradient-based optimization to the results of the direct inversion was able to significantly "clean up" the approximation, considerably reducing the dispersed softening in the solution estimation. Moreover, for this specific example, the gradient-based optimization was able to improve the relative L_2-error in the elastic modulus estimation by almost a factor of two, from a value of 6.4% after the direct inversion to a final value of 3.6%. The relative L_∞-error was reduced less significantly, going from 23.5% after direct inversion to a final value of 20.9%, but the L_∞-error is a less reliable prediction of the solution quality for localized distributions such as these, since a relatively small shift in the prediction of the inclusion location can result in a disproportionately high L_∞-error.

As a final test for this case, five trials of the inverse characterization procedure, each with a different randomly generated single-inclusion elastic modulus distribution, were performed to examine the consistency of the solution strategy. Table 1 shows the mean and standard deviation over the five random trials of the relative L_2 and L_∞ errors corresponding to the elastic modulus distributions estimated with only the direct inversion Gappy POD procedure and with the complete approach including the subsequent gradient-based optimization. The results from these random trials were highly similar to the results from the representative example shown previously. The inverse procedure was consistently able to accurately predict the elastic modulus distribution over all trials, and the gradient-based step was consistently able to significantly refine the estimation in comparison to the initial guess provided by direct inversion with a relatively small increase in computational expense when using the adjoint method for gradient calcula-

Table 1: The mean and standard deviation of the relative L_2 and L_∞ errors with respect to the elastic modulus distribution estimated with the direct inversion approach and the elastic modulus distribution estimated with the gradient-based optimization approach initialized with the direct inversion result for the five randomly generated trials with a single circular inclusion for the simulated aluminum plate example.

Approach	Relative L_2 Error		Relative L_∞ Error	
	Mean	Std. Dev.	Mean	Std. Dev.
Direct Inversion	5.5%	1.2%	27.0%	7.4%
Gradient Optimization with Direct Inversion	3.7%	1.1%	21.9%	7.2%

tions.

3.1.2. Case 2 Results: Two Circular Inclusions

The second case considered two circular inclusions within the simulated aluminum plate, and was intended to display the capabilities of the inverse solution procedure for predicting more complicated material property distributions, and particularly distributions that are fundamentally different than those used to simulate the snapshots. Furthermore, this case addresses a common inverse characterization challenge in which the property distribution may be known *priori* to be localized, but the number of localizations (e.g., damage regions) is unknown.

Fig. 5 shows a representative example of a randomly generated two-inclusion elastic modulus distribution used to simulate experimental measurements, the corresponding initial elastic modulus distribution estimation from only the direct inversion procedure (with relative L_2 and L_∞ errors of 10.1% and 33.7%), and the corresponding final elastic modulus distribution estimation from the subsequent gradient-based optimization (with relative L_2 and L_∞ errors of 8.8% and 33.6%). Similarly to the previous case, Table 2 additionally shows the mean and standard deviation over five randomly generated two-inclusion elastic modulus distribution trials of the relative L_2 and L_∞ errors corresponding to the elastic modulus distributions estimated with only the direct inversion Gappy POD procedure and with the complete approach including the subsequent gradient-based optimization. Although this case represented a considerably more challenging problem than the single-inclusion case, the inverse characterization procedure was still able to accurately estimate the elastic modulus distributions, clearly identifying two
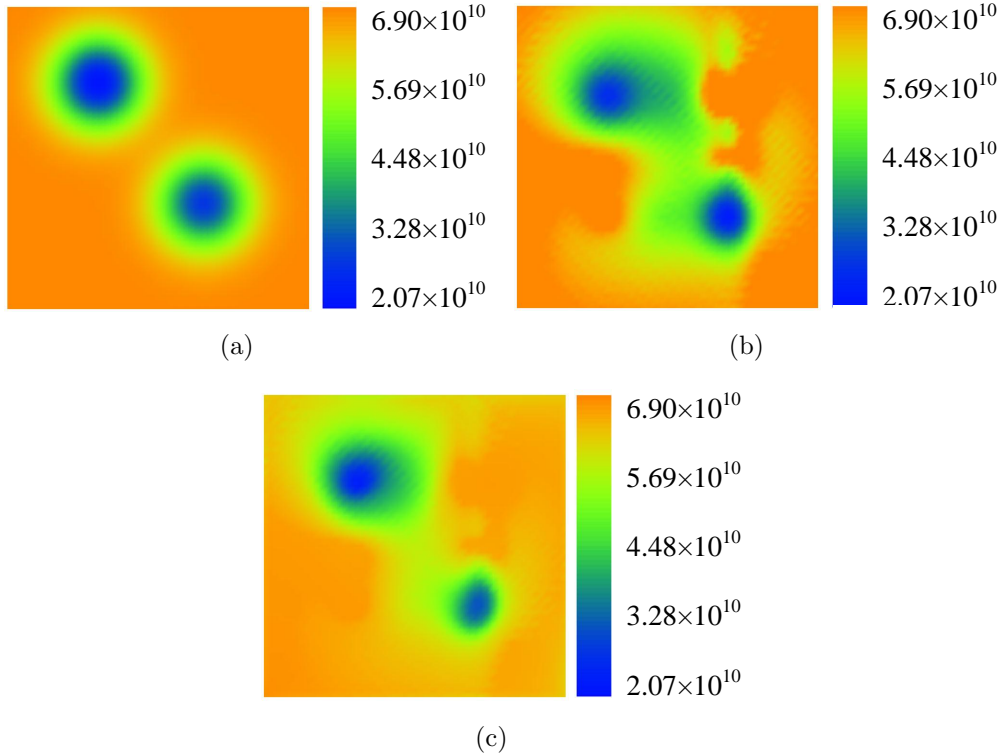
20

Figure 5: Representative two circular inclusion example of (a) the target elastic modulus distribution, (b) the elastic modulus distribution estimated with the direct inversion approach with Gappy POD full-field displacement reconstruction, and (c) the elastic modulus distribution estimated with gradient-based optimization initialized with the direct inversion solution for the simulated aluminum plate example (color contours in units of Pa).

Table 2: The mean and standard deviation of the relative L_2 and L_∞ errors with respect to the elastic modulus distribution estimated with the direct inversion approach and the elastic modulus distribution estimated with the gradient-based optimization approach initialized with the direct inversion result for the five randomly generated trials with two circular inclusions for the simulated aluminum plate example.

Approach	Relative L_2 Error		Relative L_∞ Error	
	Mean	Std. Dev.	Mean	Std. Dev.
Direct Inversion	7.6%	1.4%	32.5%	6.7%
Gradient Optimization with Direct Inversion	6.5%	1.4%	28.1%	6.5%

inclusion regions in all tests, even though the snapshot set was built only from single-inclusion scenarios. Furthermore, the gradient-based optimization continued to successfully refine the initial approximation provided by direct inversion, substantially reducing the erroneous dispersion seen in the initial estimates of the modulus distributions. However, the increase in complexity did lead to a reduction in the level of solution improvement from the gradient-based optimization, which was only able to improve the relative L_2-error of the solution estimation by approximately $10\% - 15\%$ for this case.

3.1.3. Case 3 Results: Single Irregular Inclusion

The final case for the simulated aluminum plate example explored the potential complexity of the material property distribution further by considering the presence of an irregularly shaped (i.e., non-circular) inclusion within the domain. Again, Fig. 6 shows a representative example of an elastic modulus distribution with a randomly selected irregularly shaped inclusion used to simulate experimental measurements, the corresponding initial elastic modulus distribution estimation from only the direct inversion procedure, and the corresponding final elastic modulus distribution estimation from the subsequent gradient-based optimization. Similar to the two inclusion case, the inverse characterization procedure was still able to predict an accurate final estimate to the elastic modulus distribution, even though the full-field response estimation toolset was built only from scenarios with perfectly circular inclusions and the target was irregular. However, in contrast to the two inclusion case, the gradient-based optimization step in the process led to a more substantial improvement in the inverse solution accuracy (closer to that of the single-inclusion case). In qualitative terms, the direct inversion solution appears to indicate the presence of two relatively circular inclusions in the modulus distribution, while the gradient-based refinement correctly resolves only one irregularly shaped inclusion. Moreover, the relative L_2 and L_∞ errors over the domain for the elastic modulus estimation respectively improved from 8.2% and 47.1% for the initial direct inversion estimation to 5.8% and 36.3% following gradient based optimization (i.e., an improvement in the relative L_2-error of approximately 30% and an improvement in the relative L_∞-error of approximately 23%).

3.2. Example 2: Static Test of Soft Matrix with a Hard Inclusion

To explore a different physical system and potential application, the final example consisted of a simulated 50 mm × 50 mm tissue block. The entire
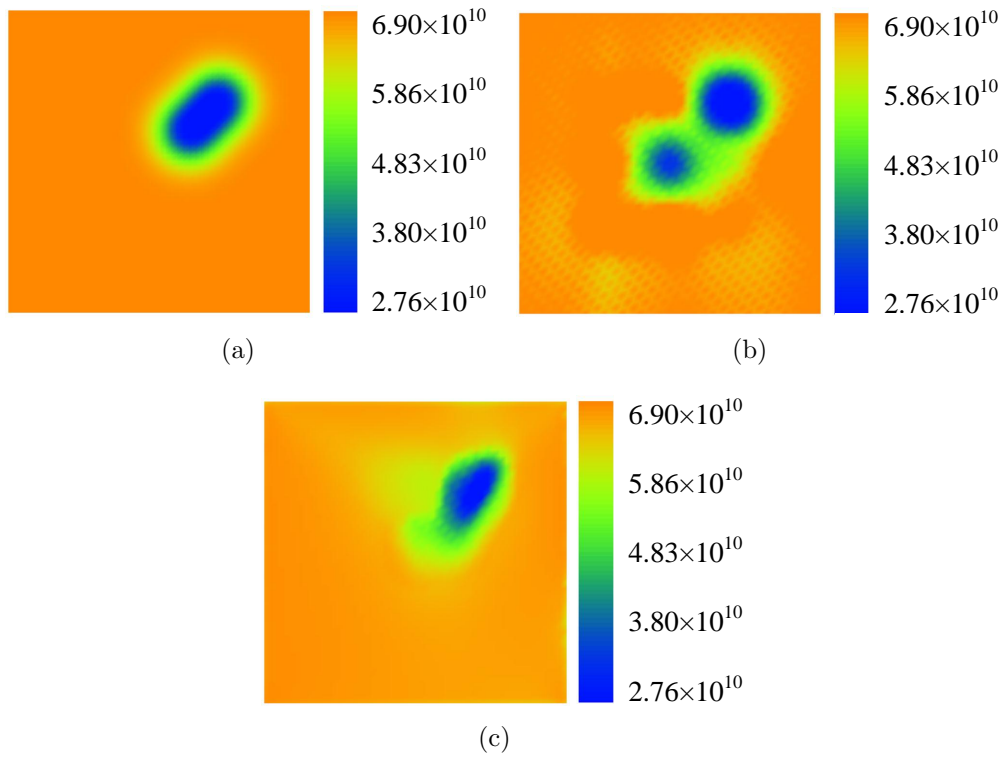
(a)

(b)

(c)

Figure 6: Representative irregular inclusion example of (a) the target elastic modulus distribution, (b) the elastic modulus distribution estimated with the direct inversion approach with Gappy POD full-field displacement reconstruction, and (c) the elastic modulus distribution estimated with gradient-based optimization initialized with the direct inversion solution for the simulated aluminum plate example (color contours in units of Pa).

material (matrix and inclusion) was assumed to be known to be nearly incompressible with a Poisson's ratio of 0.49999. For this example the simulated test was assumed to be static, with a 0.2 N/mm (factoring out the arbitrary thickness) excitation applied uniformly to the top surface of the tissue block. Note that the only difference in the formulation presented herein to convert to static rather than steady-state dynamic is that the momentum terms are set to zero. This second example scenario was intended to relate to potential applications of tissue characterization (e.g., tumor characterization) from (quasi-) static mechanical testing [10, 13].

Overall, the POD snapshot generation process was almost identical to the previous simulated aluminum plate example. Again, 37 parameter combinations were used to create the snapshots, and the same nine location combinations of a single circular RBF inclusion center were used as the first example (Fig. 2). Alternatively, the elastic modulus of the matrix (i.e., healthy) material was assumed to be fixed at 15 kPa, which was based on normal glandular breast tissue [6, 5]. The two values of the amplitude parameter used were 1 and 3 (i.e., modulus at the hard inclusion center of approximately 30 kPa and 60 kPa), and the two values of the breadth parameter used were 5 mm and 15 mm. Note that, as before, each snapshot material property distribution other than the homogeneous case contained only one inclusion. 15 out of the 37 total available POD modes were necessary to satisfy the criteria defined in Eqn. 30 and were retained for the Gappy POD reconstruction process.

3.2.1. Results: Single Irregular Inclusion

One case involving a single irregularly shaped inclusion was considered for the final simulated experiment with the statically tested tissue block. Fig. 7 shows a representative example of an elastic modulus distribution with a randomly selected irregularly shaped inclusion used to simulate experimental measurements, the corresponding initial elastic modulus distribution estimation from only the direct inversion procedure (with relative L_2 and L_∞ errors of 21.8% and 53.5%), and the corresponding final elastic modulus distribution estimation from the subsequent gradient-based optimization(with relative L_2 and L_∞ errors of 17.8% and 38.6%). Although a different mechanical testing method was considered and the properties of the system examined were substantially different, the inverse characterization results for this tissue block example were consistent with those shown for the aluminum plate example. The initial direct inversion estimation approximated the location
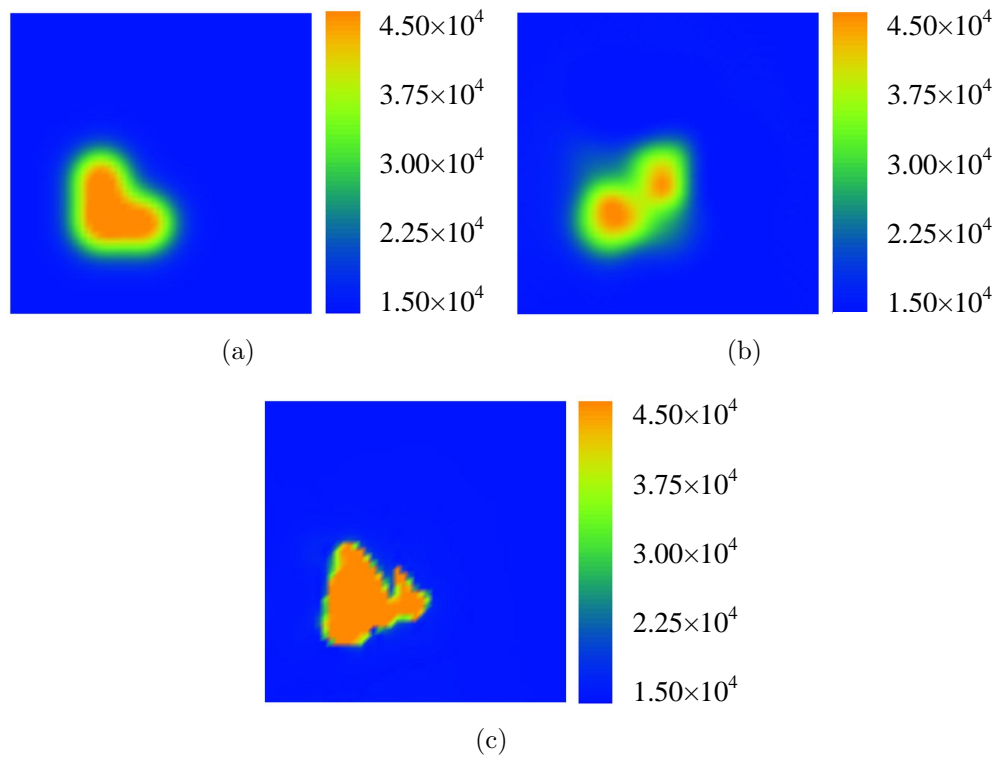
(a)

(b)

(c)

Figure 7: Representative irregular inclusion example of (a) the target elastic modulus distribution, (b) the elastic modulus distribution estimated with the direct inversion approach with Gappy POD full-field displacement reconstruction, and (c) the elastic modulus distribution estimated with gradient-based optimization initialized with the direct inversion solution for the simulated tissue block example (color contours in units of Pa).

of the inclusion relatively well, but the distribution and magnitude had significant error. Moreover, similarly to the prior test case with an irregular inclusion, although less dramatic, the initial direct inversion results appear to estimate two inclusions. The gradient-based optimization was then able to substantially improve the estimation of the elastic modulus distribution, and indicating a single irregularly shaped inclusion. One possible explanation for the slight increase in the overall solution error for this case compared to the prior test case could be the increase in the range of the elastic modulus magnitude for this tissue example. Yet, the final estimate of the elastic modulus distribution is still clearly a qualitatively accurate estimate of the location, size, and shape of the hard inclusion, which was produced at the relatively small computational cost of no more than approximately 100 finite element analyses (neglecting the one-time cost of creating the POD modes) without the need to provide a specific initial guess for the inverse solution or complicated regularization in the optimization procedure.

4. Discusions

In inverse characterization, it is appealing to use generalized parameterization (e.g., finite element-type parameterization) which doesn't require the *priori* regarding the nature of the unknown system property. However, inverse problem with high dimensionality will not only present obstacle of intractable computational cost in terms of time with global minima search algorithm (e.g., genetic algorithm), not also face the pitfall that the solution can be easily trapped in local minima with gradient adjoint approach which can track high dimensionality optimization problem but is local minima search algorithm in nature. With gradient adjoint approach, a relatively accurate initial guess of the unknown property field is necessary to ensure the success of obtaining final accurate solution. For example, as shown in Figure. 4 (b), the elastic modulus distribution was ineffectually estimated by gradient adjoint approach with a *homogeneous* (i.e., no inclusion) elastic modulus distribution in comparison to the target solution illustrated in Figure. 4 (a). Alternatively, with the initial guess provided by direct inversion with Gappy POD, the gradient adjoint approach was able to provide much more accurate estimate of elastic modulus distribution in comparison to Figure. 4 (b). The computational cost with gradient adjoint approach was solving 50 times of finite element model while the computational cost to provide good initial guess from direct inversion with Gappy POD is ap-

proximately solving 38 times finite element model. It is fascinating that a converged local minima solution can be improved significantly by solving 38 times more finite element model. Noticeably, for a given inverse characterization problem it is only necessary to complete one time snapshots generation for gappy POD algorithm which accounted 37 out of 38 times finite element solving in our direct inversion with Gappy POD, while direct inversion accounted for 1 time finite element solving. Therefore, the material property distributions of the same structure at different times in the structure's life or similar structures could be evaluated with the same set of snapshots repeatedly. Namely, the total computational cost for gradient adjoint approach with direction inversion with gappy POD will be approximately solving 51 times finite element model if material property distributions of the same or similar structure are evaluated numerous times during the structure's service life. The claim "computationally efficient" specifically implies that the inverse characterization with gradient adjoint approach can be noticeably improved with at most 38 times more finite element solving (i.e., one time structural property evaluation) and at least approximate 1 time more finite element solving (i.e., life time repeated structural property evaluation) related to direct inversion with gappy POD. To be more clear, the gradient adjoint approach with direct inversion with gappy POD provides a efficient means to initialized the starting solution of the optimization compared to normal gradient adjoint approach.

To be clarified, the contributions and novelty to combine gradient adjoint approach with direct inversion with gappy POD are not just minimal or incremental in comparison to our previous work focusing on direct inversion with gappy POD for inverse characterization [16]. The results of the numerical examples in this work have consistently shown that the solutions by gradient adjoint approach with direct inversion with gappy POD were noticeably more accurate than the solutions by direct inversion with gappy POD only. More importantly, as shown in Figure. 6 and Figure. 7, the gradient adjoint approach with direct inversion with gappy POD can more accurately estimate the irregular elastic modulus distributions while direct inversion with gappy POD can only approximate the irregular elastic modulus distributions with circular elastic modulus distributions, which were used to simplify the snapshots generation.

Worth to mentioning, the solution initial estimate by direct inversion with gappy POD only works for relatively smooth material property distribution (e.g., gaussian distribution of material property degeneration). For discontin-

uous material property distribution (e.g., cracks), the gappy POD algorithm were not able to reconstruct the response field from partial measurements accurately thus resulted in ill-posed solution of the material property estimate.

5. Conclusions

A gradient-based optimization approach for computationally efficient inverse material characterization from partial-field system response measurements capable of using a generally applicable parameterization (e.g., finite element-type parameterization) was presented and analyzed. The approach first builds a Gappy POD machine learning tool for full-field response estimation from the partial-field measurements using available *a priori* information regarding the potential unknown material property distribution. Then, a physics-based direct inversion approach with a finite element-type parameterization uses the Gappy POD estimated full-field response to produce a first estimate of the spatial distribution of the unknown material property. Lastly, the direct inversion results of the material property distribution are further refined with a gradient-based optimization strategy, which uses the adjoint method to calculate the gradients efficiently, to produce the final estimate of the material property distribution. Through numerically simulated example inverse problems based on the characterization of elastic modulus distributions with localized variations in simple structures, the inverse characterization approach was shown to efficiently estimate spatial distributions of the elastic modulus with relatively high solution accuracy from limited partial-field displacement response measurements. Furthermore, the final gradient-based optimization component was shown to be a necessary step in the characterization procedure to provide substantial and physically significant improvement in the inverse solution estimation in comparison to the direct inversion estimate alone. In addition, the complete inverse characterization approach was shown to have the capability to accurately predict material property distributions that are significantly more complicated, and particularly those that are potentially fundamentally different than the assumed material property distributions used to create the Gappy POD component. For instance, the examples presented generated the Gappy POD response estimation tool assuming elastic modulus distributions with a single perfectly circular inclusion. Yet, the inverse characterization approach was then capable of estimating elastic modulus fields with multiple inclusions

and inclusions that were irregularly shaped.

References

[1] M. Wang, J. C. Brigham, A computational nondestructive evaluation algorithm combining self-evolving parameterization and multi-objective optimization for quantitative damage characterization, Journal of Nondestructive Evaluation (2014) 1–15.

[2] G. J. Yun, K. A. Ogorzalek, S. J. Dyke, W. Song, A two-stage damage detection approach based on subset selection and genetic algorithms.

[3] J. C. Brigham, W. Aquino, F. G. Mitri, J. F. Greenleaf, M. Fatemi, Inverse estimation of viscoelastic material properties for solids immersed in fluids using vibroacoustic techniques, Journal of Applied Physics 101 (2) (2007) 023509 –023509–14.

[4] A. A. Oberai, N. H. Gokhale, M. M. Doyley, J. C. Bamber, Evaluation of the adjoint equation based algorithm for elasticity imaging, Physics in Medicine and Biology 49 (13) (2004) 2955.

[5] E. Park, A. M. Maniatty, Shear modulus reconstruction in dynamic elastography: time harmonic case, Physics in medicine and biology 51 (15) (2006) 3697.

[6] Y. Zhu, T. Hall, J. Jiang, A finite-element approach for young's modulus reconstruction, Medical Imaging, IEEE Transactions on 22 (7) (2003) 890–901.

[7] T. E. Oliphant, A. Manduca, R. L. Ehman, J. F. Greenleaf, Complex-valued stiffness reconstruction for magnetic resonance elastography by algebraic inversion of the differential equation, Magnetic resonance in Medicine 45 (2) (2001) 299–310.

[8] J. C. Brigham, W. Aquino, Surrogate-model accelerated random search algorithm for global optimization with applications to inverse material identification, Computer Methods in Applied Mechanics and Engineering 196 (45) (2007) 4561 – 4576.

[9] S. Wang, J. C. Brigham, A computational framework for the optimal design of morphing processes in locally activated smart material structures, Smart Materials and Structures 21 (10) (2012) 105016.

[10] S. Goenezen, P. Barbone, A. A. Oberai, Solution of the nonlinear elasticity imaging inverse problem: The incompressible case, Computer Methods in Applied Mechanics and Engineering 200 (13) (2011) 1406 – 1420.

[11] B. B. Guzina, M. Bonnet, Topological derivative for the inverse scattering of elastic waves, The Quarterly Journal of Mechanics and Applied Mathematics 57 (2) (2004) 161–179.

[12] G. R. Feijoo, A new method in inverse scattering based on the topological derivative, Inverse Problems 20 (6).

[13] A. A. Oberai, N. H. Gokhale, S. Goenezen, P. E. Barbone, T. J. Hall, A. M. Sommer, J. Jiang, Linear and nonlinear elasticity imaging of soft tissue in vivo: demonstration of feasibility, Physics in medicine and biology 54 (5) (2009) 1191.

[14] A. A. Oberai, N. H. Gokhale, G. R. Feijóo, Solution of inverse problems in elasticity imaging using the adjoint method, Inverse Problems 19 (2) (2003) 297.

[15] A. Sabelli, W. Aquino, A source sensitivity approach for source localization in steady-state linear systems, Inverse Problems 29 (9) (2013) 095005.

[16] M. Wang, D. Dutta, K. Kim, J. C. Brigham, A computationally efficient approach for inverse material characterization combining gappy pod with direct inversion, Computer Methods in Applied Mechanics and Engineering 286 (0) (2015) 373 – 393.

[17] S. Wright, J. Nocedal, Numerical optimization, Vol. 2, Springer New York, 1999.

[18] A. Wächter, L. T. Biegler, On the implementation of an interior-point filter line-search algorithm for large-scale nonlinear programming, Mathematical programming 106 (1) (2006) 25–57.

[19] R. Everson, L. Sirovich, Karhunen-loeve procedure for gappy data, J. Opt. Soc. Am. A 12 (8) (1995) 1657–1664.

[20] D. Venturi, G. E. Karniadakis, Gappy data and reconstruction procedures for flow past a cylinder, Journal of Fluid Mechanics 519 (2004) 315–336.

[21] M. D. Tan Bui-Thanh, K. E. Willcox, Aerodynamic Data Reconstruction and Inverse Design Using Proper Orthogonal Decomposition, AIAA Journal 42 (2004) 1505–1516.

[22] K. Willcox, Unsteady flow sensing and estimation via the gappy proper orthogonal decomposition, Computers and Fluids 35 (2) (2006) 208 – 226.

[23] A. Yakhot, T. Anor, G. Karniadakis, A reconstruction method for gappy and noisy arterial flow data, Medical Imaging, IEEE Transactions on 26 (12) (2007) 1681–1697.

[24] J. J. C. Samuel G Raben, P. P. Vlachos, Adaptive gappy proper orthogonal decomposition for particle image velocimetry data reconstruction, Measurement Science and Technology 23 (2).

[25] W. Aquino, J. Brigham, C. Earls, N. Sukumar, Generalized finite element method using proper orthogonal decomposition, International Journal for Numerical Methods in Engineering 79 (7) (2009) 887–906.

[26] B. Notghi, J. C. Brigham, Optimal nondestructive test design for maximum sensitivity and minimal redundancy for applications in material characterization, Smart Materials and Structures 22 (12) (2013) 125036.

[27] M. Contreras, S. Nagarajaiah, S. Narasimhan, Real time detection of stiffness change using a radial basis function augmented observer formulation, Smart Materials and Structures 20 (3) (2011) 035013.

[28] M. Aguilo, W. Aquino, J. Brigham, M. Fatemi, An inverse problem approach for elasticity imaging through vibroacoustics, Medical Imaging, IEEE Transactions on 29 (4) (2010) 1012–1021.

[29] C. Compas, E. Wong, X. Huang, S. Sampath, B. Lin, X. Papademetris, D. Dione, A. Sinusas, M. O'Donnell, J. Duncan, Radial basis functions for combining shape and speckle tracking in 4d echocardiography.

[30] MathWorks, Matlab r2012a documentation, MATLAB R2012a Documentation.